First-principles calculations of the electronic structure and phase stability of Ni-Mo alloys

1998 J. Phys.: Condens. Matter 10 8459

(http://iopscience.iop.org/0953-8984/10/38/007)

J. Phys.: Condens. Matter **10** (1998) 8459–8475. Printed in the UK PII: S0953-8984(98)91603-4

First-principles calculations of the electronic structure and phase stability of Ni–Mo alloys

A Arya†, G P Das‡, S Banerjee† and M J Patni§

† Materials Science Division, Bhabha Atomic Research Centre, Mumbai 400085, India
‡ TP & PE Division, Bhabha Atomic Research Centre, Mumbai 400085, India
§ Department of Metallurgical Engineering and Materials Science, Indian Institute of Technology, Mumbai 400076, India

Received 12 February 1998, in final form 12 May 1998

Abstract. Self-consistent local density electronic structure calculations have been carried out on various fcc-based ground-state ordered superstructures of $Ni_{1-x}Mo_x$ alloys spanning the entire concentration range. Using the tight-binding linear muffin-tin orbital (TB-LMTO) method, we have calculated the volume-dependent total ground-state energies, and hence the different equilibrium cohesive properties, as functions of the Mo concentration. Following the 'transferability prescription' of Andersen and co-workers, we have estimated the potential parameters of the constituent atoms as embedded in the alloy and compared these with the corresponding charge-self-consistent parameters for the intermetallic compounds. The ground-state stability profile has been obtained for the first time for this family of Ni–Mo compounds. Moreover, we have tested the applicability of the cluster expansion method (CEM) for parametrizing the cohesive energies to estimate the volume-dependent effective cluster interactions (ECIs) under the octahedron–tetrahedron cluster approximation.

1. Introduction

The electronic structures of ordered as well as substitutionally disordered binary alloys have been the subject of much theoretical and experimental investigation in recent years [1, 2]. Such studies have two aims, namely that of (a) designing alloys with the desired strength and ductility [3] and that of (b) achieving an understanding of the phase stability and order–disorder transformations in alloys. The latter, in particular, has come to a stage of maturity, because of the advent of a number of theoretical and computational tools to describe the configurational thermodynamics in metallic alloys. The basic idea is to evaluate the ground-state energy of an alloy as a function of its concentration, configuration and volume, by using some efficient electronic structure total-energy method, such as the tight-binding linear muffin-tin orbital (TB-LMTO) method [4–6] used here. This method can be used in conjunction with (a) the cluster expansion method (CEM) [7], (b) the coherent potential approximation (CPA) and its generalizations [8, 9] or (c) the augmented-space recursion (ASR) method [10, 11], in order to extract the effective many-body interactions. Subsequently, the configurational entropy contribution at finite temperature can be calculated using statistical mechanical methods, such as the cluster variation method (CVM) [12–14] and the static-concentration-wave (SCW) method [15, 16].

0953-8984/98/388459+17$19.50

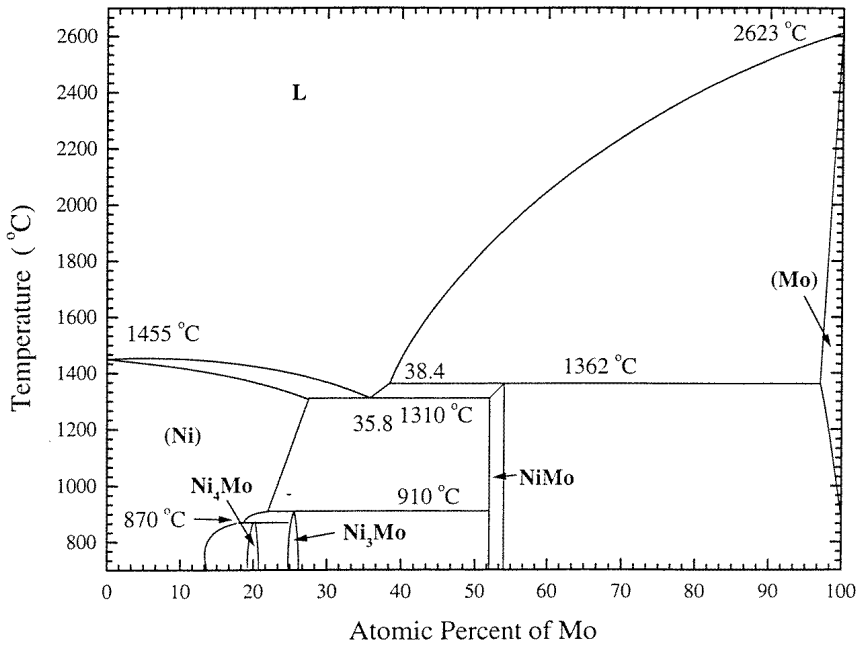

Figure 1. The experimental Ni–Mo phase diagram (taken from reference [19]).

We have recently applied the LDA-based TB-LMTO-CEM approach to investigate the ground-state phase stability of Li–Al alloys under the first- and the second-nearest-neighbour pair approximation [17, 18]. In the present paper, we have extended our studies to transition-metal-based (TM-based) intermetallics and determined the various electronic and cohesive properties and the ground-state stability profile, and also estimated the volume-dependent (but concentration-independent) effective multi-site interactions. We have chosen a typical TM-based binary alloy, namely Ni–Mo, which has several equilibrium ordered intermetallic phases [19] (see figure 1), namely the β-phase (Ni_4Mo), the γ-phase (Ni_3Mo) and the δ-phase (NiMo), and metastable phases such as Ni_2Mo (Pt_2Mo-type structure), Ni_3Mo (DO_{22}) and Ni_2Mo_2. This alloy family is particularly interesting from the point of view of studying the relative stability of these *competing* fcc-based ordered intermetallic phases (superstructures). Although the phase transformation behaviour of these alloys has been extensively studied using several experimental techniques, there has been no attempt to investigate their electronic and cohesive properties using a first-principles theoretical approach which can serve as a precursor to studying their ordering behaviour. Here, we report the results of our LDA electronic structure total-energy calculations for all of the fcc-based ordered superstructures of the Ni–Mo system (see table 1). For each structure and composition, we estimate the equilibrium cell volume, bulk modulus, cohesive energy and compound formation energy, and thereby arrive at the zero-temperature stability sequence. We have also tested the applicability of the cluster expansion prescription to obtain the volume-dependent effective multi-site/cluster interactions (ECI), by taking into consideration those structures which can be stabilized up to the second-nearest-neighbour pair approximation. Finally, we discuss the electronic structures of these stable compounds in terms of their DOSs, potential parameters and site- and l-projected partial charges.

Table 1. The crystallographic data for various fcc-based ground-state superstructures under the first- and the second-nearest-neighbour pair interactions. The transformed basis vectors are given in terms of the vectors of the fcc lattice.

Structures	Compositional formulae	Space group symbol (No)	Wyckoff positions	Multi-plicity	Transformed basis
fcc based					
A1	A	$Fm\bar{3}m$ (225)	A (a)	4	$\boldsymbol{a} = a\{100\}$
$L1_0$	AB	$P4/mmm$ (123)	A (a)	1	$\boldsymbol{a}_1 = \frac{1}{2}a\{110\}$
			B (d)	1	$\boldsymbol{a}_2 = \frac{1}{2}a\{1\bar{1}0\}$
					$\boldsymbol{c} = a\{001\}$
$L1_1$	AB	$R\bar{3}m$ (166)	A (a)	1	$\boldsymbol{a}_1 = \frac{1}{2}a\{110\}$
			B (b)	1	$\boldsymbol{a}_2 = \frac{1}{2}a\{101\}$
					$\boldsymbol{c} = a\{222\}$
A_2B_2	A_2B_2	$I4_1/amd$ (141)	A (a)	4	$\boldsymbol{a}_1 = a\{010\}$
			B (b)	4	$\boldsymbol{a}_2 = a\{001\}$
					$\boldsymbol{c} = a\{200\}$
Pt_2Mo	A_2B	$Immm$ (71)	A (i)	4	$\boldsymbol{a} = \frac{1}{2}a\{1\bar{1}0\}$
			B (a)	2	$\boldsymbol{b} = a\{001\}$
					$\boldsymbol{c} = \frac{1}{2}a\{330\}$
$L1_2$	A_3B	$Pm\bar{3}m$ (221)	A (c)	3	$\boldsymbol{a} = a\{100\}$
			B (a)	1	
DO_{22}	A_3B	$I4/mmm$ (139)	A (d)	4	$\boldsymbol{a}_1 = a\{010\}$
			A (b)	2	$\boldsymbol{a}_2 = a\{001\}$
			B (a)	2	$\boldsymbol{c} = a\{200\}$
$D1_a$	A_4B	$I4/m$ (87)	A(h)	8	$\boldsymbol{a}_1 = \frac{1}{2}a\{3\bar{1}0\}$
			B(a)	2	$\boldsymbol{a}_2 = a\{130\}$
					$\boldsymbol{c} = \{002\}$
hcp based					
DO_a	A_3B	$Pmmn$ (59)	B (a)	2	
			A (b)	2	
			A (f)	4	

2. Computational details

Electronic structure calculations have been performed using the first-principles TB-LMTO method [4–6], which combines the simplicity of the TB approach with an accuracy comparable to that of the Korringa–Kohn–Rostoker (KKR) method. This method has undergone substantial development in the past decade, as can be seen from the recent review [20]. For close-packed metallic systems, the simplifying atomic sphere approximation (ASA) [21] has proved to be quite successful. In the case of binary intermetallics, if there is considerable size difference between the two constituents (as in the Ni–Mo system under consideration here), it is desirable to ensure that the overlap between the atomic

spheres of radii s_1 and s_2, defined as $100(s_1 + s_2 - d)/s_1$ [6], remains less than ∼30%. The errors due to the neglect of the interstitial region and truncation of higher partial waves are minimized by incorporating the so-called 'combined correction' terms. According to Andersen, the ASA with the combined correction should yield reasonably accurate results, especially for close-packed intermetallics [6] for which the wavelength of the interstitial solution turns out to be rather large.

The matrix elements of the one-electron Hamiltonian in a nearly orthogonal LMTO basis can be written as

$$H_{\boldsymbol{R}L,\boldsymbol{R}'L'} = C_{\boldsymbol{R}L}\delta_{\boldsymbol{R}\boldsymbol{R}'}\delta_{LL'} + \Delta^{1/2}_{\boldsymbol{R}L}[S^0(1-\gamma S^0)^{-1}]_{\boldsymbol{R}L,\boldsymbol{R}'L'}\Delta^{1/2}_{\boldsymbol{R}'L'} \tag{1}$$

where $\boldsymbol{R}$ is the site index and L is the angular momentum index (l, m), with $l \leqslant 2$ (i.e. s, p and d partial waves on all of the atoms) for the present calculations. S^0 is the canonical structure constant matrix, which depends on the structure of the underlying fcc lattice, but is independent of the lattice constant and which type of atoms occupy the sites. The properties of the atoms which occupy the lattice sites are characterized by the parameters C, Δ and γ, which depend only on the potentials in the spheres at $\boldsymbol{R}$ and are therefore called *potential parameters*. The self-consistent potential parameters are generated by solving the scalar-relativistic radial Schrödinger equation at the sphere boundary and its energy derivative at the reference energies E_ν characteristic of the linear method. We have used the von Barth–Hedin parametrization [23] of the exchange–correlation potential in our local density band calculations. The hopping integrals in the above Hamiltonian depend on the potential around each atom and therefore indirectly on the interatomic distances. In the TB-LMTO method, further simplification is achieved by the use of the so-called screened structure constant matrix (S^α) and a localized basis set ($|\chi^\alpha\rangle$) which is highly sensitive to the different local chemical rearrangements of the underlying (here fcc) lattice. The screening transformation can be defined as [4]

$$|\chi^\alpha\rangle = |\chi^0\rangle(1+\alpha S^\alpha) \qquad \text{where } S^\alpha = S^0(1-\alpha S^0)^{-1}. \tag{2}$$

It has been extensively used for calculating the ground-state properties of close-packed metallic systems. The resulting self-consistent potential parameters for s-, p-, d- and f-electron elements have been tabulated in the literature [5].

For A_xB_{1-x} binary alloys obeying Vegard's law, the volume per atom V^0_{alloy} in the alloy is simply the concentration-weighted average of the normal-pressure atomic volumes of the constituents V^0_{M} (M = A or B); i.e.,

$$xV^0_{\text{A}} + (1-x)V^0_{\text{B}} = V^0_{\text{alloy}}. \tag{3}$$

The use of normal-pressure values of the constituent's potential parameters yields a sufficiently accurate potential and charge density. However, for alloys showing deviation from Vegard's law, the potentials of the elements should be calculated at such a pressure that the concentration-weighted sum of the atomic volumes equals the actual volume per atom in the alloy. The assumption of the pressure–volume relation yields [6]

$$\frac{(V_{\text{A}} - V^0_{\text{A}})}{V^0_{\text{A}}} : \frac{(V_{\text{B}} - V^0_{\text{B}})}{V^0_{\text{B}}} = \frac{\beta^0_{\text{B}}}{\beta^0_{\text{A}}} \tag{4}$$

where β^0_{M} (M = A, B) are the bulk moduli of the pure components. The solution of equation (3) and equation (4) yields the volumes of the constituents:

$$\begin{aligned} V_{\text{A}} &= \frac{\beta^0_{\text{B}}V_{\text{alloy}} + (1-x)V^0_{\text{B}}(\beta^0_{\text{A}} - \beta^0_{\text{B}})}{xV^0_{\text{A}}\beta^0_{\text{B}} + (1-x)V^0_{\text{B}}\beta^0_{\text{A}}}V^0_{\text{A}} \\ V_{\text{B}} &= \frac{\beta^0_{\text{A}}V_{\text{alloy}} + (1-x)V^0_{\text{A}}(\beta^0_{\text{B}} - \beta^0_{\text{A}})}{xV^0_{\text{A}}\beta^0_{\text{B}} + (1-x)V^0_{\text{B}}\beta^0_{\text{A}}}V^0_{\text{B}}. \end{aligned} \tag{5}$$

Table 2. Calculated equilibrium ground-state properties of various ordered intermetallic phases of the Ni–Mo alloy system. (e/a denotes the electron-to-atom ratio.)

Structures, fcc based	e/a	s_{av} (s_{Ni}, s_{Mo}) (au)	Bulk modulus (GPa)	E_{coh} (kJ mol^{-1})	E_{form} (kJ mol^{-1})
Ni (fcc)	10.0	2.500	256.268	−791.563	0.0
Ni_4Mo	9.2	2.636 (2.543, 2.952)	298.232	−878.942	−25.322
Ni_3Mo (DO_a)	9.0	2.656 (2.542, 2.951)	299.484	−894.154	−25.021
Ni_3Mo ($L1_2$)	9.0	2.662 (2.548, 2.957)	248.609	−876.189	−7.055
Ni_3Mo (DO_{22})	9.0	2.653 (2.539, 2.947)	258.678	−893.540	−24.406
Ni_2Mo	8.67	2.691 (2.540, 2.948)	258.011	−927.099	−32.109
NiMo ($L1_0$)	8.0	2.757 (2.538, 2.946)	91.586	−971.583	−24.879
Ni_2Mo_2	8.0	2.788 (2.568, 2.978)	208.916	−961.409	−14.705
NiMo ($L1_1$)	8.0	2.790 (2.570, 2.980)	334.423	−969.644	−22.940
$NiMo_2$	7.33	2.842 (2.555, 2.964)	242.533	−1008.604	−10.186
$NiMo_3$ ($L1_2$)	7.0	2.856 (2.539, 2.947)	225.490	−1050.957	−26.682
$NiMo_3$ (DO_{22})	7.0	2.862 (2.545, 2.953)	255.108	−1042.724	−18.450
Mo (fcc)	6.0	2.959	279.411	−1101.845	0.0
Mo (bcc)	6.0	2.959	283.902	−1140.265	0.0

So the potential parameters in the alloy for the component M (A or B) should be calculated at the new radius $s_M = (3V_M/4\pi)^{1/3}$. The values of the potential parameters at the radii appropriate to the alloy phase, s_M, can be obtained from the normal-pressure radii s_M^0 and the volume derivatives of the potential parameters using the logarithmic interpolation formulae [6]

$$\begin{aligned} C &= C^0 + \frac{\mathrm{d}C}{\mathrm{d}\ln s}\ln(s/s^0) \\ \gamma &= \gamma^0 + \frac{\mathrm{d}\gamma}{\mathrm{d}\ln s}\ln(s/s^0) \\ \Delta &= \Delta^0\left[\frac{s}{s^0}\right]^{\mathrm{d}\ln\Delta/\mathrm{d}\ln s} \\ (p)^{-1/2} &= (p^0)^{-1/2}\left[\frac{s}{s^0}\right]^{\mathrm{d}\ln(p)^{-1/2}/\mathrm{d}\ln s}. \end{aligned} \tag{6}$$

Here $(p)^{-1/2}$ is a measure of the energy window inside which a linear method is supposed to yield realistic results. This parameter is usually small in magnitude and is not very important.

The volume derivatives of the potential parameters used above have been tabulated [5] for all of the elements.

After extrapolation of the potential parameters to the new radii, one must take into account the fact that the alloy Wigner–Seitz (WS) radius is different from that of the pure components, where the WS radii are the same as the sphere radii. This affects only two of the parameters, namely Δ and γ, which should be multiplied by $(s_M/W)^{(2l+1)}$, where $W = (3V_{alloy}/4\pi)^{1/3}$ is the alloy WS radius; i.e.,

$$(\Lambda)_{alloy} = (s/W)^{2l+1}(\Lambda)_{pure\ component} \qquad \text{where } \Lambda = \Delta, \gamma. \tag{7}$$

The prescription (5) for obtaining the sphere radii for the components in an alloy usually leads to only a small charge transfer between the spheres, and has been successfully used for a number of intermetallic systems (see, for example, reference [22]). The corresponding potential parameters obtained using the logarithmic interpolation formulae are found to be in reasonably good agreement with those obtained from charge-self-consistent calculations for the ordered alloys, provided that the system does not deviate too much from the Vegard's-law criterion. In this work, we have employed the above-mentioned 'transferability' prescription of Andersen *et al* [6], as can be seen in the following section.

3. Results and discussion

3.1. Stability of ground-state superstructures

The Ni–Mo phase diagram [19] shows three ordered intermetallic phases on the Ni-rich side, namely the β-phase (Ni_4Mo), the γ-phase (Ni_3Mo) and the δ-phase (NiMo). $Ni_{1-x}Mo_x$ alloys are known to be non-magnetic for $x \geqslant 0.12$, and therefore we have neglected any magnetic contribution in our present treatment. For our theoretical investigation, we have considered 12 fcc-based *coherent* structures† (see table 1), apart from the two equilibrium structures, namely Mo (bcc) and the Ni_3Mo (DO_a) structure. The hcp-based Ni_3Mo (DO_a) structure is the only hcp-based structure included here, because in the 75:25 composition, this is the stable structure closely competing with the related fcc-based DO_{22} structure. These two structures are generated, respectively, by ABAB... and ABCABC... stacking sequences of similar close-packed planes. These 14 structures include all of the stable or metastable phases in this system.

The crystallographic information for all of the above-mentioned structures is summarized in table 1. Each of these structures is a superstructure of the parent fcc lattice; i.e., they are formed because of different chemical arrangements of the constituent atomic species. But the lattice of the atomic sites remains cubic. We have performed self-consistent (non-spin-polarized) calculations for global minimization of the total ground-state energy with respect to the cell volume, keeping $c/a = 1$. The equilibrium WS radii for the pure constituents (table 2) are found to be in reasonably good agreement with the experimental values [24] ($s_{Ni} = 2.602$ au, $s_{Mo} = 2.928$ au), as well as with the KKR [25] ($s_{Ni} = 2.561$ au, $s_{Mo} = 2.912$ au) and ASW [26] ($s_{Ni} = 2.589$ au, $s_{Mo} = 3.005$ au) calculations. For each of the ordered compounds, if we choose equal-sized atomic spheres of the constituent atoms, the charge transfer from Mo to Ni is found to be rather large. However, the compressibility criterion (mentioned in section 2) yields different atomic sphere radii for Ni and Mo constituents for each superstructure, which are given in table 2, along with

† These are the ground-state superstructures, under the first- and second-nearest-neighbour approximation, in the entire concentration range. At 50:50 concentration, we have considered the fcc-based Ni_2Mo_2 (metastable) and the $L1_0$ and $L1_1$ phases, instead of the δ-phase NiMo which is a complex hcp superstructure.

Table 3. The number of valence electrons (Q_l) inside the atomic (WS) spheres, partitioned according to the angular momentum, for fcc-based superstructures of the Ni–Mo alloy system. The Q_{sph}-values are the fractional numbers of electrons inside the Ni and the Mo spheres, as embedded in the respective compounds. The weighted sum of these sphere charges yields the total valence charge (Q_T) in the compound.

Phase	Ni				Mo				$N(E_F)$ (states
(Φ)	Q_{sph}	Q_s	Q_p	Q_d	Q_{sph}	Q_s	Q_p	Q_d	(Ryd atom)$^{-1}$)
Ni (fcc)	10.0	0.648	0.756	8.596	—	—	—	—	52.692
Ni_4Mo	10.015	0.666	0.761	8.588	5.940	0.662	0.831	4.447	23.051
Ni_3Mo	10.032	0.683	0.765	8.584	5.918	0.643	0.823	4.452	12.160
(DO_a)	10.024	0.674	0.770	8.580	—	—	—	—	
Ni_3Mo ($L1_2$)	10.017	0.663	0.778	8.576	5.951	0.651	0.790	4.510	37.658
Ni_3Mo	10.019	0.663	0.776	8.580	5.927	0.649	0.821	4.457	14.360
(DO_{22})	10.036	0.673	0.775	8.588	—	—	—	—	
Ni_2Mo	10.020	0.674	0.769	8.577	5.961	0.647	0.802	4.512	8.829
NiMo ($L1_0$)	10.031	0.677	0.794	8.560	5.969	0.650	0.758	4.561	15.391
NiMo ($L1_1$)	9.927	0.673	0.775	8.579	5.973	0.681	0.746	4.546	14.731
Ni_2Mo_2	10.014	0.684	0.766	8.564	5.986	0.651	0.761	4.574	21.429
$NiMo_2$	9.908	0.686	0.769	8.553	5.996	0.665	0.758	4.573	18.262
$NiMo_3$ ($L1_2$)	10.056	0.688	0.826	8.542	5.982	0.654	0.754	4.574	11.786
$NiMo_3$	10.029	0.685	0.795	8.549	5.978	0.654	0.768	4.556	15.826
(DO_{22})	—	—	—	—	6.015	0.660	0.740	4.615	
Mo (fcc)	—	—	—	—	6.000	0.656	0.762	4.582	14.946
Mo (bcc)	—	—	—	—	6.000	0.644	0.834	4.522	7.353

the corresponding equilibrium WS radius (s_{av}). These sets of values of s_{Ni} and s_{Mo} ensure equally good sphere packing for all of the structures under consideration and at the same time yield *more or less charge-neutral* spheres, as can be seen from table 3. The sphere charges (Q_{sph}) deviate from the corresponding elemental values by $\leqslant 0.7\%$ for Ni and $\leqslant 1.6\%$ for Mo. The equilibrium s_{av}-values are found to be slightly higher (systematically) than the corresponding Vegard's-law values, although the numbers follow the same increasing trend with increasing Mo concentration—i.e. with decreasing ratio e/a (figure 2). This small positive deviation from Vegard's law is a manifestation of solid-solution effects in Ni–Mo alloys.

Table 2 also summarizes other calculated cohesive properties, namely bulk moduli, cohesive energies and formation energies of these superstructures. The bulk moduli (β), obtained from the second derivative of the total energy with respect to volume, remain more or less the same, lying within a narrow band (see figure 3) for all of the structures; NiMo ($L1_0$) is the only exception, for which it abruptly drops by a factor of 3. The calculated values for the pure components are comparable with the corresponding ASW results [26]—

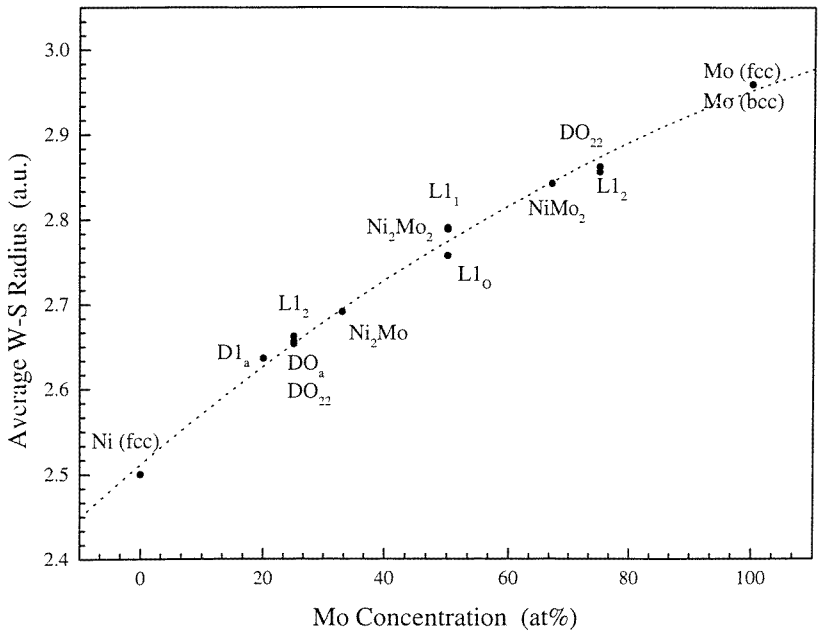

Figure 2. The average Wigner–Seitz radii of the ordered Ni–Mo compounds plotted as a function of the Mo concentration. The continuous curve has been drawn to indicate the trend in equilibrium volume per atom with concentration.

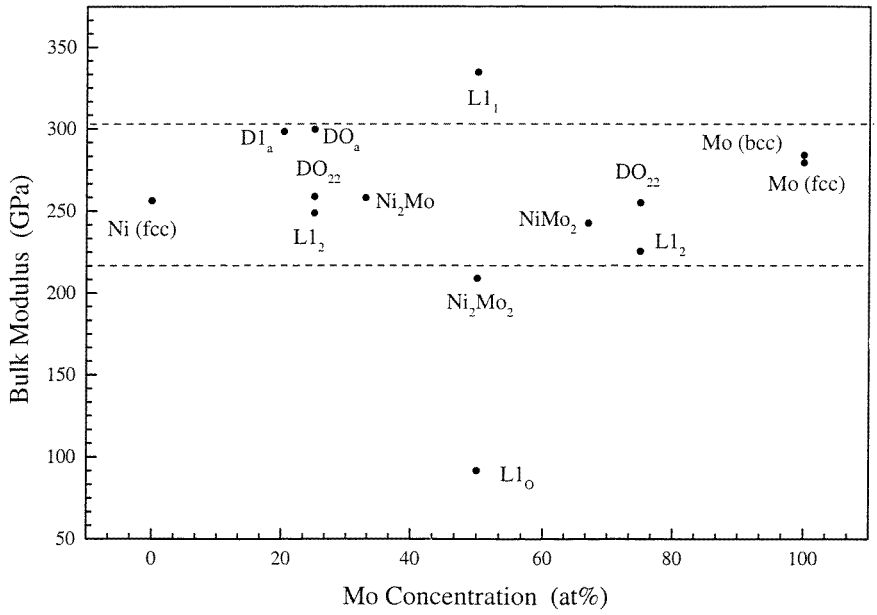

Figure 3. The calculated bulk moduli for various Ni–Mo compounds plotted as a function of the Mo concentration.

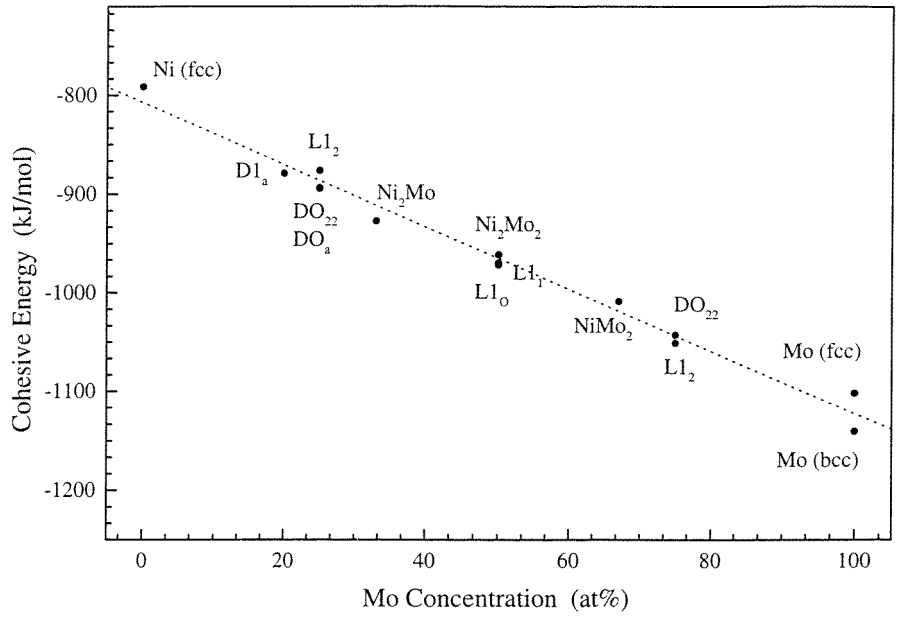

Figure 4. The calculated cohesive energies of Ni–Mo compounds plotted as a function of the valence electron/atom ratio.

namely, $\beta_{\mathrm{Ni(fcc)}} = 260$ GPa, $\beta_{\mathrm{Mo(fcc)}} = 230$ GPa and $\beta_{\mathrm{Mo(bcc)}} = 250$ GPa.

From the ASA total energy [5], we have calculated the cohesive energy (E_{coh}) for each superstructure by subtracting the weighted sum of total atomic energies. Our calculated E_{coh}-values are found to increase with increasing Ni concentration (i.e. e/a increasing), as can be seen from table 2 and figure 4†. The KKR values for the cohesive energies of Ni (fcc) and Mo (bcc), as quoted in the literature [25], are respectively -0.413 Ryd (i.e. -541.995 kJ mol^{-1}) and -0.495 Ryd (i.e. -649.606 kJ mol^{-1}). Our calculated cohesive energy values (table 2) are found to be systematically overestimated. This is partly due to the use of the ASA and partly due to the subtle difference between the manners in which the atomic calculations are performed [25, 17]. Here we have performed the free-atom calculations semi-relativistically, using the same computer code as was used for our solid calculations, but with a large cut-off $r_{max} = 30$ au. The resulting total free-atom energies are -3037.080 Ryd for Ni and -8090.228 Ryd for Mo, the corresponding KKR values being -3011.233 Ryd and -7946.087 respectively [25]. The saving grace is that the systematic errors in our cohesive energy values are more or less cancelled for close-packed metallic systems, when we calculate their formation energies as [13]

$$E^{\mathrm{fcc}}_{form}(\mathrm{Ni}_{1-x}\mathrm{Mo}_x) = E^{\mathrm{fcc}}_{coh}(\mathrm{Ni}_{1-x}\mathrm{Mo}_x) - (1-x)E^{\mathrm{fcc}}_{coh}(\mathrm{Ni}) - xE^{\mathrm{fcc}}_{coh}(\mathrm{Mo}). \tag{8}$$

The energy of formation of a given *fcc-based* coherent superstructure has been calculated with respect to the pure fcc-based non-magnetic constituents [13], although fcc Mo is not the equilibrium structure and fcc Ni is ferromagnetic‡.

† We have followed the thermodynamic convention of quoting E_{coh} as a negative quantity; this is in conformity with the definition of compound formation energy which should be negative for a stable structure.

‡ The difference between the total-ground-state-energy values of ferromagnetic and non-magnetic Ni is found to be only ∼3 mRyd from our calculations.

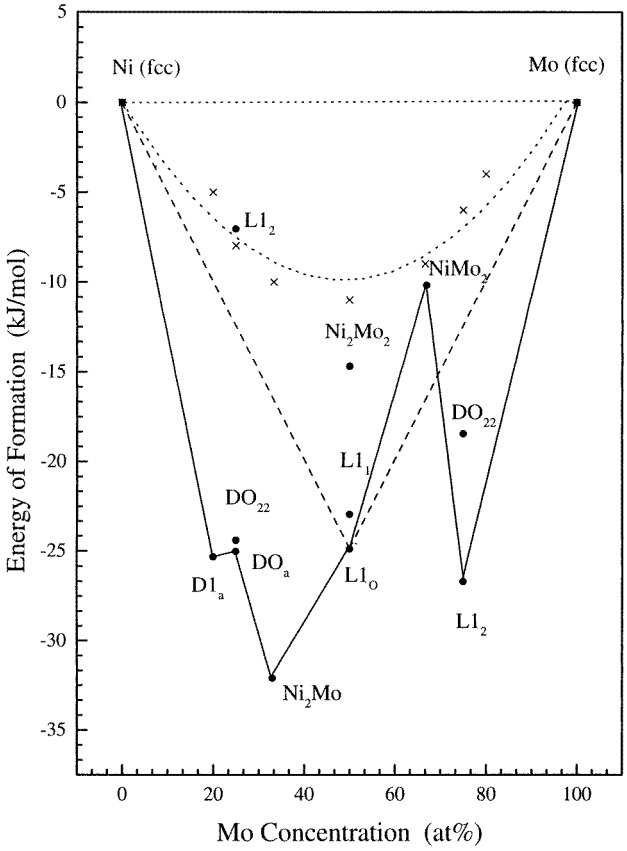

Figure 5. The calculated energies of formation of Ni–Mo compounds as a function of the Mo concentration. The solid lines join the most stable structures at the respective compositions. The dotted parabola is fitted to the heats of formation (crosses) as predicted by Miedema's semi-empirical formula.

Our calculated E_{form}-values as a function of composition have been plotted in figure 5, and superposed onto these are results of Miedema's semi-empirical predictions [27]. For the 50:50 composition, the $L1_0$ phase has the lowest value of E_{form}—i.e., the highest stability. On the Ni-rich side, the E_{form}-values for Ni_4Mo ($D1_a$), Ni_3Mo (DO_a) and Ni_2Mo all lie below the 'mechanical-mixture line' (the short-dashed line in figure 5) joining NiMo ($L1_0$) and pure Ni (fcc), signifying that these are the stable/metastable phases for the respective compositions. For $x_{Mo} = 0.25$, the values of E_{form} for the hcp-based DO_a and the fcc-based DO_{22} structures are found to be very close, although the former is more stable, as is also confirmed by experiments [28, 29]. A similar argument, extended to the Mo-rich side, shows $NiMo_3$ ($L1_2$) to be the stable structure, while $NiMo_3$ (DO_{22}) is metastable.

3.2. Calculation of ECIs for Ni–Mo alloys

Apart from obtaining the zero-temperature phase stability of different Ni_xMo_{1-x} ordered superstructures, it is possible to use the self-consistent TB-LMTO ground-state energies, in conjunction with the CEM, to obtain the *configuration-independent* ECIs. The procedure

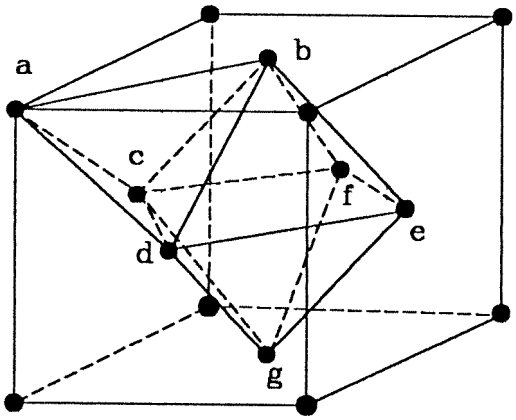

Figure 6. The octahedron (bcdefg)–tetrahedron (abcd) cluster approximation for the fcc lattice.

Table 4. The coefficients of the effective (multi-site) interaction ($j_\gamma^{(k)}$) for the fcc Ni–Mo alloys under the octahedron–tetrahedron approximation. Successive clusters $\gamma = 0, 1, \ldots, 10$ are, respectively, as follows: empty (0), point (1), nearest-neighbour (NN) pair (2), next-nearest-neighbour (NNN) pair (3), equilateral NN triangle (4), 2NN–1NNN isosceles triangle (5), equilateral tetrahedron (6), 5NN–1NNN irregular tetrahedron (7), 4NN–2NNN square (8), pyramid (9) and octahedron (10). The unit for calculation of J_γ is kJ mol^{-1}.

γ	$j_\gamma^{(0)}$	$j_\gamma^{(1)}$	$j_\gamma^{(2)}$	$J_\gamma(V)$ ($V = 8.033$ cm^3 mol^{-1})
0	100.495	−262.673	16.610	−937.402
1	−162.879	8.854	3.628	142.257
2	282.021	−73.954	5.373	34.619
3	−188.718	41.787	−2.327	−3.209
4	−96.604	17.348	−0.772	−7.063
5	68.353	0.073	−0.514	35.761
6	−196.473	50.701	−3.257	0.606
7	258.692	−58.233	3.409	10.908
8	−95.698	27.638	−1.926	2.049
9	66.703	−14.699	0.785	−0.721
10	−33.593	6.900	−0.329	0.631

has been discussed in our earlier work on Li–Al alloys [17, 18]. We have used here the *octahedron–tetrahedron* cluster approximation for the fcc lattice (figure 6) which accounts for pair interactions up to the second-nearest neighbour and gives rise to 11 subclusters (including the maximal cluster). In order to determine the interactions via the CEM, one therefore needs a set of 11 fcc-based ordered structures. Accordingly, we have taken the self-consistent values of E_{coh} of only 11 fcc-based structures (Ψ), symmetrically distributed over the entire concentration range (e.g. A, A_3B, A_2B, AB, AB_2, AB_3 and B)†. The corresponding cluster correlation functions (ξ_γ^Ψ) form an 11×11 matrix which can easily be inverted to yield the ECIs, given the cohesive energies (from our LDA calculations) of the ordered superstructures. By expanding these volume-dependent cohesive energies

† We have ignored the $D1_a$ structure for the time being, because stability of this structure can be achieved only if one considers interactions up to at least fourth-nearest neighbours.

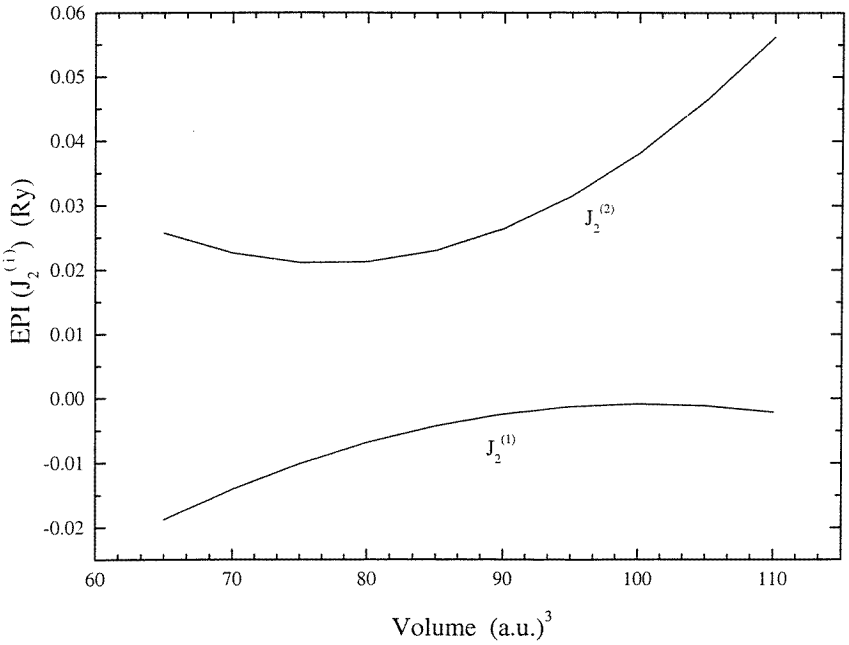

Figure 7. The effective pair interactions for the first- and the second-nearest-neighbour pairs ($J_2^{(1)}$ and $J_2^{(2)}$), calculated using the CEM, plotted as a function of the volume.

around the equilibrium volume V_0, and retaining terms up to second order, we get the ECIs as

$$J_\gamma(V) = j_\gamma^{(0)} + j_\gamma^{(1)} V + j_\gamma^{(2)} V^2. \tag{9}$$

Table 4 summarizes the calculated coefficients for the volume expansion ($j_\gamma^{(k)}$, $k = 0, 1, 2$) of the ECIs, which on substitution in equation (5) yield the values of $J_\gamma(V)$ for a typical value of V. The unexpectedly large magnitude of the values of $J_\gamma(V)$ for the irregular triangle and tetrahedron ($\gamma = 5$ and 7, respectively) may be attributed to the fact that these are rather unphysical subclusters [30]. The effective pair interactions for the first- and the second-nearest-neighbour pairs ($J_2^{(1)}$ and $J_2^{(2)}$) as a function of volume have been plotted in figure 7. As a cross-check on the reliability of these J_γ-values for Ni–Mo alloys, we have substituted these ECIs back into the cluster expansion

$$E_{coh}^{\Psi}(V) = \sum_\gamma J_\gamma(V) \xi_\gamma^{\Psi} \tag{10}$$

and the fitted cohesive energy values so obtained match (within $\pm 3\%$) those obtained from our LDA calculations for these superstructures.

3.3. Electronic structure and chemical bonding

In view of the fact that there are neither any band-structure calculations nor any relevant experimental data which have been reported in the literature on the $Ni_{1-x}Mo_x$ intermetallics, we shall try to bring out the systematic trends in their electronic properties as obtained from our self-consistent LDA investigation. Another objective of this section is to discuss and

Table 5. The potential parameters for the various coherent phases of the Ni–Mo system as calculated using the charge-self-consistent TB-LMTO method. The corresponding WS radii values have been taken from table 2.

Phase	Potential parameters									
	Ni					Mo				
(ϕ)	$s^{\phi}_{\mathrm{Ni}}/s^{\phi}_{av}$	C	Δ	$1/\sqrt{p}$	γ	$s^{\phi}_{\mathrm{Mo}}/s^{\phi}_{av}$	C	Δ	$1/\sqrt{p}$	γ
Ni	1.0	−0.307	0.198	5.217	0.427		—	—	—	—
(fcc)		0.792	0.184	6.984	0.114		—	—	—	—
		−0.156	0.013	0.788	−0.003		—	—	—	—
Mo		—	—	—	—	1.0	−0.165	0.171	4.985	0.437
(fcc)		—	—	—	—		0.852	0.166	5.473	0.125
		—	—	—	—		0.001	0.031	1.392	0.018
Ni_4Mo	0.965	−0.304	0.192	5.229	0.412	1.120	−0.199	0.192	5.068	0.490
($D1_a$)		0.796	0.166	6.948	0.102		0.824	0.235	5.551	0.176
		−0.165	0.011	0.792	−0.002		−0.063	0.054	1.403	0.034
Ni_3Mo	0.957	−0.305	0.190	5.191	0.409	1.111	−0.193	0.191	5.090	0.487
(DO_a)		0.793	0.161	6.916	0.100		0.831	0.229	5.541	0.172
		−0.165	0.011	0.790	−0.002		−0.056	0.052	1.403	0.032
	0.957	−0.304	0.191	5.205	0.409		—	—	—	—
		0.795	0.162	6.921	0.100		—	—	—	—
		−0.164	0.011	0.790	−0.002		—	—	—	—
Ni_3Mo	0.957	−0.301	0.191	5.255	0.409	1.111	−0.187	0.192	5.114	0.487
(DO_{22})		0.803	0.162	6.962	0.100		0.842	0.231	5.537	0.172
		−0.163	0.011	0.797	−0.002		−0.049	0.053	1.411	0.032
	0.957	−0.298	0.192	5.257	0.409		—	—	—	—
		0.807	0.162	6.968	0.100		—	—	—	—
		−0.154	0.011	0.798	−0.002		—	—	—	—
Ni_2Mo	0.944	−0.299	0.189	5.239	0.403	1.096	−0.185	0.189	5.080	0.480
(*Immm*)		0.804	0.155	6.946	0.096		0.841	0.221	5.528	0.165
		−0.158	0.010	0.797	−0.002		−0.042	0.049	1.410	0.030
NiMo	0.920	−0.295	0.184	5.230	0.393	1.069	−0.174	0.185	5.082	0.468
($L1_0$)		0.806	0.144	6.906	0.089		0.855	0.206	5.504	0.153
		−0.151	0.009	0.798	−0.002		−0.023	0.044	1.411	0.026
$NiMo_2$	0.899	−0.306	0.177	5.118	0.383	1.043	−0.181	0.178	4.966	0.456
(*Immm*)		0.782	0.132	6.791	0.082		0.832	0.187	5.496	0.142
		−0.160	0.008	0.783	−0.002		−0.023	0.038	1.382	0.023
$NiMo_3$	0.889	−0.286	0.178	5.233	0.380	1.032	−0.166	0.179	5.067	0.451
($L1_2$)		0.814	0.129	6.880	0.079		0.862	0.184	5.498	0.138
		−0.138	0.008	0.800	−0.001		−0.010	0.037	1.412	0.022

test the transferability of the LMTO potential parameters from the pure components to the alloy according to the prescription of Andersen *et al* [6] as discussed in section 2.

For the sake of brevity, we have restricted consideration to those structures which show maximum stability (see section 3.1) for a given composition—namely, Ni_4Mo ($D1_a$), Ni_3Mo (DO_a), NiMo ($L1_0$) and $NiMo_3$ ($L1_2$), in addition to Ni_3Mo (DO_{22}) which closely competes with DO_a. Table 5 summarizes our charge-self-consistent potential parameters

Table 6. The potential parameters for various coherent phases of the Ni–Mo system calculated using the logarithmic interpolation formulae (see the text for details).

	Potential parameters							
	Ni				Mo			
Phase	C	Δ	$1/\sqrt{p}$	γ	C	Δ	$1/\sqrt{p}$	γ
Ni_4Mo	−0.309	0.192	5.269	0.413	−0.162	0.193	5.028	0.490
($D1_a$)	0.795	0.166	6.940	0.103	0.861	0.234	5.486	0.175
	−0.176	0.011	0.791	−0.002	0.001	0.056	1.405	0.032
Ni_3Mo	−0.308	0.191	5.277	0.409	−0.160	0.192	5.035	0.486
(DO_a)	0.797	0.162	6.939	0.100	0.863	0.228	5.486	0.171
	−0.175	0.011	0.792	−0.002	0.002	0.054	1.408	0.031
Ni_3Mo	−0.305	0.191	5.301	0.409	−0.157	0.193	5.055	0.486
(DO_{22})	0.804	0.163	6.936	0.100	0.870	0.229	5.486	0.171
	−0.172	0.011	0.796	−0.002	0.005	0.054	1.414	0.031
Ni_2Mo	−0.306	0.189	5.292	0.404	−0.158	0.190	5.048	0.479
($Immm$)	0.801	0.156	6.937	0.096	0.868	0.220	5.486	0.164
	−0.173	0.010	0.795	−0.002	0.004	0.050	1.412	0.029
NiMo	−0.304	0.184	5.308	0.394	−0.156	0.185	5.062	0.467
($L1_0$)	0.806	0.145	6.936	0.089	0.872	0.204	5.486	0.152
	−0.171	0.009	0.797	−0.002	0.006	0.045	1.416	0.026
$NiMo_2$	−0.320	0.177	5.190	0.384	−0.173	0.178	4.959	0.456
($Immm$)	0.771	0.133	6.950	0.083	0.838	0.187	5.486	0.141
	−0.186	0.008	0.778	−0.002	−0.009	0.039	1.383	0.022
$NiMo_3$	−0.305	0.178	5.299	0.380	−0.157	0.179	5.054	0.451
($L1_2$)	0.803	0.131	6.937	0.080	0.869	0.184	5.486	0.137
	−0.172	0.007	0.796	−0.001	0.005	0.037	1.414	0.021

(namely C, Δ, $1/\sqrt{p}$ and γ) obtained using the s_{Ni}- and s_{Mo}-values given by the Vegard's-law values of the WS radii for Ni and Mo (see table 2). Since all of the intermetallic structures under consideration here are close packed and the deviation from Vegard's law is marginal, it is expected that these sets of potential parameters should match with those obtained via the transferability scheme (table 6). In the latter scheme, we simply take the calculated values of the potential parameters of the pure elements at the equilibrium WS radii, and scale them to those corresponding to the alloy WS radii via the logarithmic interpolation formulae. The logarithmic derivatives of the potential parameters have been taken from reference [5]. The overall agreement of these potential parameters with the charge-self-consistent ones in table 5 testifies to the validity of the transferability prescription used. These near-neutral sphere potential parameters can also be used for the electronic structure calculations of disordered alloys [22], where lattice relaxation plays a crucial role. Note that for some structures, such as DO_a and DO_{22}, there are two types of Ni atom in the Ni-rich alloys, whose average values can only be compared with the corresponding entries of table 6. The minor discrepancies (in mRyd range) can be attributed to (a) the equilibrium cell volumes deviating from the Vegard's-law values and (b) the charge transfer and consequent Madelung potentials in the alloy which cannot be accounted for in the results obtained using the transferred parameters. However, we have found that these small discrepancies do not affect the DOSs calculated for the two sets of

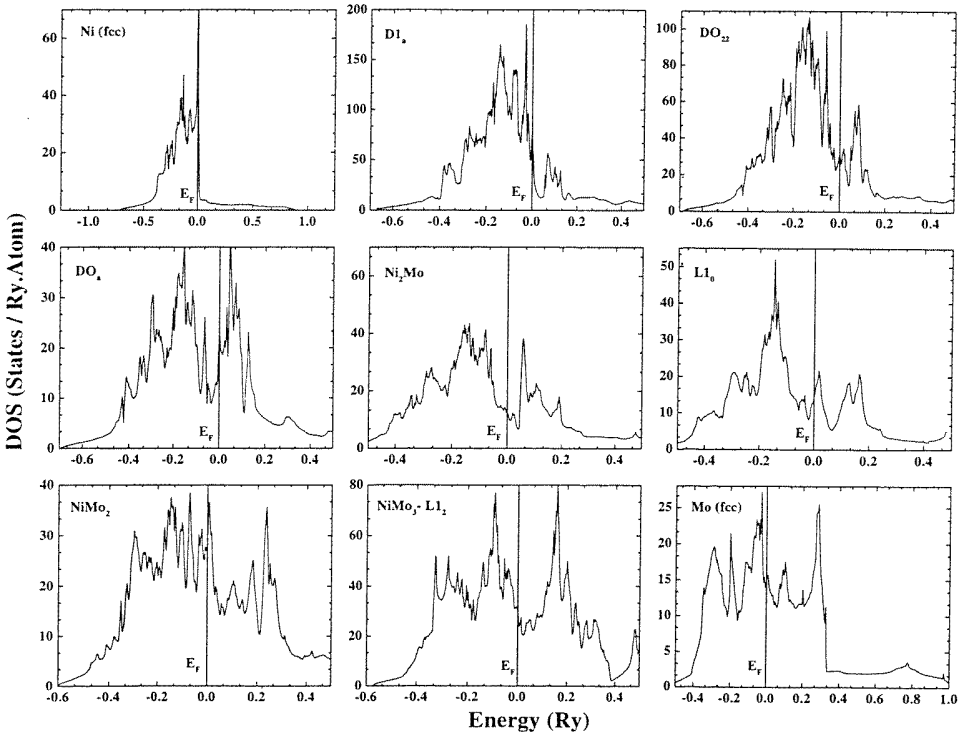

Figure 8. The total densities of states of different stable and metastable structures of Ni–Mo intermetallics.

potential parameters.

Total DOSs for all the lowest-energy ordered structures (including those for Ni (fcc) and Mo (fcc)) as calculated via the self-consistent TB-LMTO method are shown in figure 8. The occupied part of the DOS reveals a multi-peaked structure for almost all of the Ni_xMo_{1-x} compounds, which clearly show the transition from a Mo-like DOS (with a nearly half-filled d band having an occupied bandwidth of ∼0.5 Ryd) to a Ni-like DOS (with a nearly filled d band having an occupied bandwidth of ∼0.7 Ryd).

The fractional l-decomposed charges (Q_l) obtained from the ASA calculations (see table 3) depend on the sphere radii used and hence cannot be interpreted as the inter-site charge transfer. However, for a fixed composition, since we have used the same value of $s_{\mathrm{Ni\,(Mo)}}/s_{av}$ around both Ni and Mo sites, it should be possible to estimate the *intra*-site promotion of electrons and also the relative trend in the inter-site (more appropriately inter-sphere) charge transfer. For example, if we compare the Q_{sph}-values for Ni_3Mo in the DO_a, $L1_2$ and DO_{22} structures, we observe that maximum charge is transferred from Mo to Ni in the DO_a structure, which also turns out to be the most stable one for this 75:25 composition.

Another important quantity is the DOS at the Fermi level, $N(E_F)$, which is used for estimation of the electronic specific heat and the electron–phonon coupling constant, and even for determining the vibrational contribution to the entropy at finite temperature. It is observed (table 3) that $N(E_F)$ is a minimum for the lowest-energy superstructure at a particular composition.

4. Summary

The various cohesive properties and the zero-temperature structure stability of a series of ordered $Ni_{1-x}Mo_x$ compounds have been obtained from first-principles TB-LMTO electronic structure calculations. We have considered only fcc-based ground-state superstructures which are stabilized within the second-nearest-neighbour pair approximation. This ground-state stability analysis has shown the DO_a, $L1_0$ and $L1_2$ structures to be the most stable for the 75:25, 50:50 and 25:75 concentrations, respectively. The hcp-based DO_a structure ($E_{form} = -25.021$ kJ mol^{-1}) closely competes with the fcc-based DO_{22} structure ($E_{form} = -24.406$ kJ mol^{-1}), in agreement with experimental observations. Our zero-temperature stability analysis also predicts Ni_2Mo (Pt_2Mo-type structure) to have the highest stability (figure 5). Even though this Ni_2Mo phase does not appear in the experimental phase diagram, there is experimental evidence, based on transmission electron microscopy [28, 29], which suggests that this phase does form during the quenching of the alloys containing 8–33% Mo from higher temperatures (ranging between 600 and 800 °C. We are therefore inclined to believe that a mixture of Ni_3Mo and NiMo phases perhaps has lower free energy than the Ni_2Mo phase. The trends in the charge transfers, as well as the values of the DOS at E_F, conform to the stability sequence obtained. The cohesive energies of 11 fcc-based ordered structures have been used in conjunction with the cluster expansion prescription for obtaining the ECIs as a function of cell volume. The convergence of the cluster expansion has also been analysed.

The WS radius of Mo is about 12% larger than that of Ni, and the equilibrium values for the various intermetallic compounds are also found to be somewhat larger than the corresponding Vegard's-law values. We have therefore used the prescription of Andersen *et al* to estimate the 'correct' volumes of the constituent atoms as embedded in particular intermetallic compounds, and hence calculated the new renormalized potential parameters via the logarithmic interpolation formulae, involving volume derivatives. These 'transferred' potential parameters match the corresponding charge-self-consistent results reasonably well, thereby attesting to the validity of the prescription used. In fact, these potential parameters can be used immediately for the corresponding disordered Ni–Mo alloys, which undergo lattice relaxation due to appreciable size difference between Ni and Mo atoms.

Acknowledgments

This work forms a part of the PhD project, carried out at the Indian Institute of Technology, Mumbai, of one of the authors (AA). The authors are grateful to Professor A Mookerjee for many helpful discussions.

References

[1] Pettifor D G and Cottrell A H 1992 *Electron Theory in Alloy Design* (London: The Institute of Materials)
[2] Ducastelle F 1991 *Order and Phase Stability in Alloys* (New York: North-Holland)
[3] Paxton A T and Pettifor D G 1992 *Scr. Metall.* **26** 529
[4] Andersen O K and Jepsen O 1984 *Phys. Rev. Lett.* **53** 2571
[5] Andersen O K, Jepsen O and Glötzel D 1985 *Highlights in Condensed Matter Theory* ed F Bassani, F Fumi and F M Tosi (Amsterdam: North-Holland) p 59
Note: a complete set of LMTO potential parameters, along with the volume derivatives, for all of the elements in the periodic table, has been calculated by Kumm A E 1992 *PhD Thesis* University of Stuttgart
[6] Andersen O K, Jepsen O and Šob M 1987 *Electronic Band Structure and its Applications (Springer Lecture Notes in Physics 283)* ed M Yussouff (Berlin: Springer) p 1

[7] Connolly W and Williams A R 1983 *Phys. Rev.* B **27** 5169
Connolly W and Williams A R 1984 *The Electronic Structure of Complex Systems* ed W Temmerman and P Phariseau (New York: Plenum) p 581
[8] Stocks G M, Gyorffy B L, Giuliano E S and Ruggeri R 1977 *J. Phys. F: Met. Phys.* **7** 1859
[9] Kudrnovský J and Drchal V 1990 *Phys. Rev.* B **41** 7515
[10] Mookerjee A 1990 *J. Phys.: Condens. Matter* **2** 897
Mookerjee A 1990 *J. Phys.: Condens. Matter* **2** 9399
[11] Mookerjee A 1994 *Methods of Electronic Structure Calculations* ed V Kumar, O K Andersen and A Mookerjee (Singapore: World Scientific) and references therein
[12] Sanchez J M and de Fontaine D 1978 *Phys. Rev.* B **17** 2926
[13] Sluiter M, de Fontaine D, Guo X Q, Podloucky R and Freeman A J 1990 *Phys. Rev.* B **42** 10 460
[14] Morita T, Suzuki M, Wada K and Kaburagi M (ed) 1994 *Prog. Theor. Phys. Suppl.* **115**
[15] Khachaturyan A G 1978 *Prog. Mater. Sci.* **22** 1
[16] Khachaturyan A G 1983 *Theory of Structural Transformations in Solids* (New York: Wiley)
[17] Arya A, Das G P, Salunke H G and Banerjee S 1994 *J. Phys.: Condens. Matter* **6** 3389
[18] Das G P, Arya A and Banerjee S 1996 *Intermetallics* **4** 625
[19] Massalski T B (ed) 1990 *Binary Alloy Phase Diagrams* (Materials Park, OH: ASM International)
[20] Andersen O K, Jepsen O and Krier G 1994 *Lectures on Methods of Electronic Structure Calculations* ed V Kumar, O K Andersen and A Mookerjee (Singapore: World Scientific) p 63
[21] Andersen O K 1975 *Phys. Rev.* B **12** 3060
[22] Bose S K, Kudrnovský J, Jepsen O and Andersen O K 1992 *Phys. Rev.* B **45** 8272
[23] von Barth U and Hedin L 1972 *J. Phys. C: Solid State Phys.* **5** 1629
[24] Villars P and Calvert L D 1985 *Pearson's Handbook of Crystallographic Data for Intermetallic Phases* (Metals Park, OH: American Society for Metals)
[25] Moruzzi V L, Janak J F and Williams A R 1978 *Calculated Electronic Properties of Metals* (New York: Pergamon)
[26] Moruzzi V L and Sommers C B 1995 *Calculated Electronic Properties of Ordered Alloys* (Singapore: World Scientific)
[27] de Boer F R, Boom R, Mattens W C M, Miedema A R and Niessen A K 1988 *Cohesion in Metals: Transition Metal Alloys* (Amsterdam: North-Holland)
[28] Kulkarni U D and Banerjee S 1988 *Acta Metall.* **36** 413
[29] van Tendeloo G, Amelinckx S and de Fontaine D 1985 *Acta Crystallogr.* B **41** 281
[30] Sanchez J M 1996 private communication